AIMS Energy, 12(1): 235–255.
DOI: 10.3934/energy.2024011
Received: 11 December 2023
Revised: 04 January 2024
Accepted: 19 January 2024
Published: 29 January 2024

http://www.aimspress.com/journal/energy

*Research article*

# Investigation of various hybrid nanofluids to enhance the performance of a shell and tube heat exchanger

**Ruaa Al Mezrakchi***

Department of Engineering, College of Science and Engineering, University of Houston-Clear Lake, Houston, Texas 77058, USA

* **Correspondence:** Email: almezrakchi@uhcl.edu; Tel: +12812833828.

**Abstract:** In this study, we aim to investigate the heat transfer and flow characteristics of diverse hybrid nanofluids (CuO-ZnO-Water, EG-Water, CuO-EG-Water, $SiO_2$-EG-Water, and $Al_2O_3$-EG-Water) as coolants across eight discrete inlet velocities in a shell and tube heat exchanger. Various materials (copper, stainless steel, titanium, and carbon steel) have been employed for the tubing to optimize system performance. The impact of Reynolds number concerning hybrid nanofluids on Nusselt number and friction factor was assessed in this research. The results of the numerical simulations are found to agree well with experimental results within an average deviation of 1.8%. The results indicated the superior heat transfer capabilities of the hybrid nanofluid compared to the base fluid across all conditions. The outcomes revealed the superior heat transfer capabilities of the CuO-ZnO-Water hybrid nanofluid under all tested conditions. When employing CuO-ZnO-Water as a coolant, a substantial increase of over 9% in temperature reduction was observed, as opposed to the approximately 6% attained by other hybrid nanofluids at a lower velocity of 0.5 m/s. Notably, higher Reynolds numbers corresponded to increased Nusselt numbers and decreased friction factors. The decline percentage of the friction factor was 43% at Reynolds number ranging between 10,000 to 40,000. We emphasize the imperative need to optimize nanoparticle types for crafting hybrid nanofluids to enhance the performance of industrial heat exchangers and their coolant efficiency. Ultimately, the utilization of hybrid nanofluids in conjunction with shell and tube heat exchanger systems has yielded a notable enhancement in the overall thermal efficiency of these systems.

**Keywords:** nanofluids; heat transfer; shell and tube heat exchanger; nanoparticles; friction factor; Nusselt number; SOLIDWORKS

## 1. Introduction

Heat exchangers for decades have been extensively employed across diverse industrial applications as crucial agents for heat transfer. Heat exchangers serve the pivotal function of transferring heat between different mediums, encompassing gases, liquids, or their combinations. This technology substantially enhances energy efficiency by redirecting surplus heat to other systems capable of utilizing this energy effectively. A tangible illustration of this process occurs in the real-world scenario of harnessing the exhaust from an electricity-producing gas turbine, channeling it through a heat exchanger to generate steam for driving a secondary steam turbine, thereby amplifying electricity generation. Additionally, heat exchangers find widespread application in pre-heating cold fluids entering a heated process system, leveraging the heat from a warmer fluid exiting the system, thereby curtailing the energy input required to elevate the incoming fluid to operational temperatures [1,2].

Various applications highlight the utility of heat exchangers, including heating a cooler fluid using the heat from a hotter fluid, cooling a hot fluid by transferring its heat to a cooler fluid, boiling a liquid using the heat from a hotter fluid, boiling a liquid while condensing a hotter gaseous fluid, and condensing a gaseous fluid by means of cooler fluid. The fluid dynamics within heat exchangers typically involve rapid flow to expedite heat transfer via forced convection. Assessing the efficacy of heat exchangers entails gauging their ability to transfer heat in relation to the pressure losses incurred by the fluids due to swift flow. Contemporary heat exchanger designs prioritize minimizing pressure drops while maximizing heat transfer and accommodating additional design criteria such as fluid pressures, prevention of fouling or corrosion, and ensuring simplicity in maintenance and repair procedures [2–6].

The analysis of diverse heat exchanger configurations with varying parameters is rooted in the principles of the first and second laws of thermodynamics. Under the assumption of steady-state flow and adiabatic conditions, the first law simplifies to heat input equating heat output, providing a foundational framework for heat exchanger design. The second law remains the guiding principle, asserting that heat naturally flows from a higher-temperature body to a lower-temperature one, a fundamental premise dictating heat exchanger operations. In these systems, the colder fluid gains heat from the hotter fluid, causing an increase in its temperature while reducing the temperature of the hotter fluid [7–9].

Continuous efforts have been devoted to augmenting heat exchangers' efficiency, incorporating various strategies such as the integration of fins [10,11] and porous materials [12,13] to amplify surface area, the introduction of baffles in diverse shapes to induce turbulence [14–16], the implementation of rough surfaces [17,18], and the substitution of conventional coolant with nanofluids [19,20]. Among these methodologies, nanofluids which are the mixture of water and nanoparticles with different concentrations. Nanofluids can be employed for the cooling of automobile engines and welding equipment, as well as for managing high heat-flux apparatus such as high power microwave tubes and high-power laser diode arrays. The utilization of nanofluid coolant in various systems has aimed at enhancing its operational efficiency. Moreover, the assessment of critical heat transfer enhancement via nanofluids proved advantageous for nuclear applications, and encompassed a broad spectrum of industries, spanning from transportation to energy production involving electronic systems like microprocessors, micro-electro-mechanical-systems MEMS, and within the realm of biotechnology [21]. These nanofluids have exhibited considerable promise in ameliorating heat exchanger performance across a wide spectrum of parameters encompassing nanoparticle concentration, inlet temperature, Reynolds number, and Prandtl number without necessitating alterations to the existing heat exchanger

setup. Subsequent enhancement of the thermophysical properties of the base fluid through the addition of nanoparticles with higher thermal conductivity led to modifications in the heat transfer performance of the heat exchanger [22,23].

Despite the evolution in the development of new nanoparticle types, only a limited range of nanoparticles has been studied to assess their impact on the performance of heat exchanger systems. Thus, this research delved into investigate the specific operational mechanisms of heat exchangers with the influence of various types of nanoparticles embedded into heat exchanger fluids forming nanofluid subsystem. Computational models validated with experiments were used as a foundation to explore different types of nanofluids, and thus optimize the performance of the heat exchanger system accordingly. Shell and tube heat exchanger configurations were adopted as a case study to explore variations in the thermophysical properties exhibited by the nanofluids involved. In the scrutiny of a shell and tube heat exchanger, a multitude of design variables could come under evaluation. These encompass flow rates, the thermal attributes linked to inlet and outlet temperatures, the system's pressure dynamics, the consequential pressure drop, factors influencing resistance, the inherent physical traits characterizing the fluids, and the dimensions defining the shell and tube geometry. The comprehensive assessment of these parameters forms the cornerstone of optimizing the efficacy and performance of heat exchange systems.

## 2. Model design and simulation

In the pursuit of creating a functional shell and tube heat exchanger, we undertook the comprehensive development of the overall design. This investigation was conducted through numerical analysis employing SOLIDWORKS Flow Simulation software. Each constituent element underwent meticulous design procedures and subsequent assembly to actualize the cohesive formation of the heat exchanger system.

### *2.1. Overall design and attributes*

An external view of the heat exchanger design, highlighting the fusion of the shell and headers, is illustrated in Figure 1a. With dual headers, one serving as the inlet and the other as the outlet, the design simplicity allows seamless integration into various systems. Figure 1b,c illuminate the internal dynamics of the heat exchanger, revealing the anticipated flow behavior of distinct fluids.

Primarily constituting the foundational structure, the shell of the heat exchanger was the initial component to be meticulously crafted. Its pivotal role encompassed the encapsulation of all subsequent components. Figure 1 illustrates the top inlet and bottom outlet of the shell, housing the coolant fluid volume while accommodating the internal construction of other elements. The shell's comprehensive specifications encompassed the following parameters: A length of 0.6000 m, an outer diameter of 0.1300 m, an inner diameter of 0.1250 m, stainless steel material, and an inlet & outlet hole diameter of 0.0137 m.

The design incorporated tubes intended for central insertion within the shell, complemented by affixed baffles. Depicted in Figure 1b and Figure 1c, each tube, totaling eight in number, adhered to a specific pattern configuration with calculated pitch spacing. These tubes were affixed to the header, housing the flow volume of a more abrasive fluid. The tube's specifications comprised a length of 0.6000 m, an outer diameter of 0.0137 m, an inner diameter of 0.0107 m, a total of 8 tubes, a pitch spacing of 0.0182 m,

and a material composition of copper.

Functioning as terminations on both ends of the shell, the headers, as displayed in Figure 1b and Figure 1c, were a dual installation in the overall system. The inlet or outlet point, depending on its placement, utilized a small orifice. The key specifications of the header design included a curvature radius of 0.0650 m, a length of 0.0500 m, a diameter of 0.1300 m, an inlet & outlet hole diameter of 0.0137 m, and a material made of stainless steel.

The integration of baffles within the shell served the purpose of channeling or restricting the flow of distinct fluids. Figure 1b and Figure 1c delineate three baffle designs. Two baffles located at either end adjacent to the connecting header, functioned to segregate fluids and direct flow through the shell-encased tubes. While third designed baffles evenly dispersed within the shell strategically cut on opposing sides for enhanced directional performance. The baffle specifications included a diameter of 0.1250 m, a thickness of 0.0100 m, a hole diameter of 0.0137 m, and a baffle spacing of 0.15 m.

The strategic placement of headers coupled with baffle implementation delineates a path for fluid flow, optimizing heat distribution across the pipes. The three additional baffles, configured to facilitate 25% horizontal flow, guide fluid movement around and over the pipes, enhancing heat distribution efficiency.

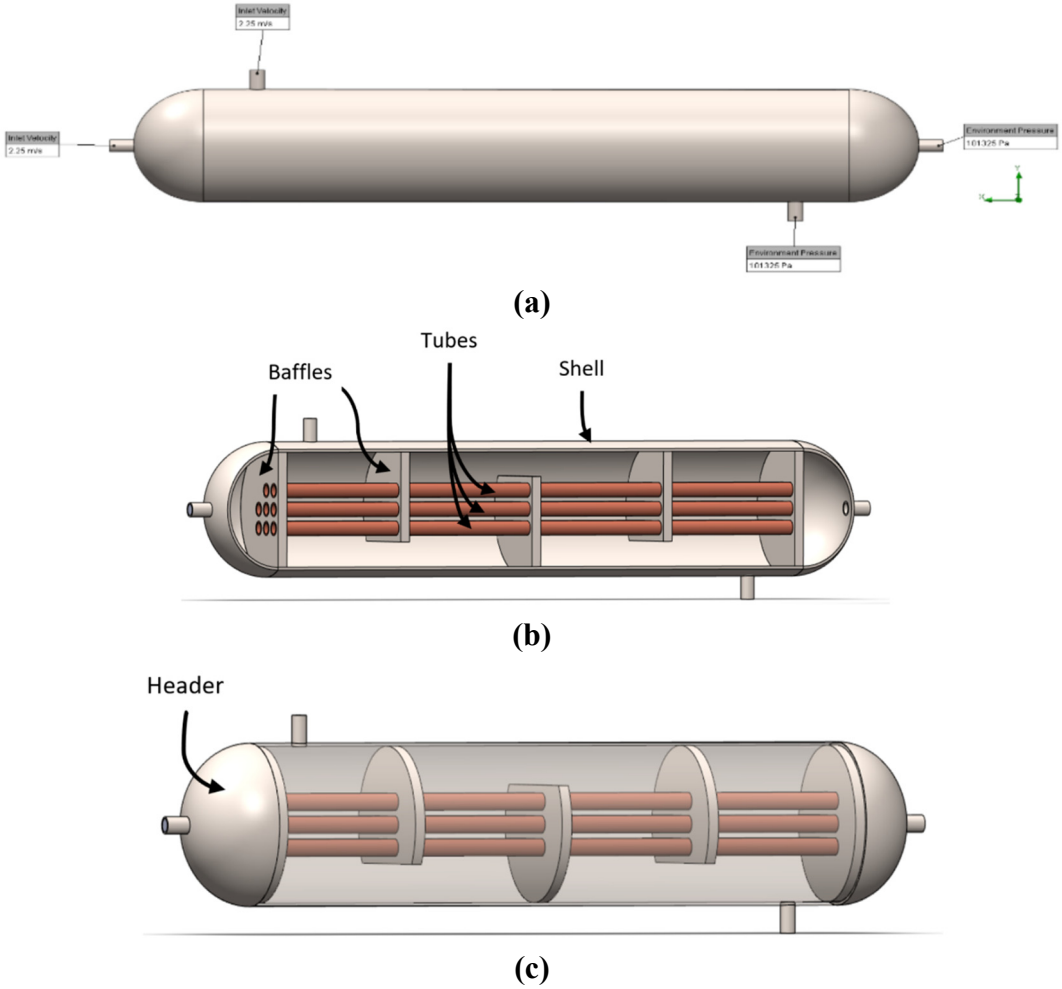


**Figure 1.** Design of heat exchanger: (a) overall external view, (b) internal view with introduced cut, (c) internal view with shell transparent.

### *2.2. Material and nanofluid parameters*

The material parameters corresponding to the distinct materials utilized in the heat exchanger design are presented in Table 1 [24,25]. The strategic use of these materials simplifies the simulation and analysis phases of the research, focusing primarily on assessing different nanofluids employed as cooling agents. The inherent strengths and thermal properties of these materials are tabulated in Table 1, forming the basis for theoretical calculations and numerical analysis. Furthermore, the properties of six distinct coolant nanofluids slated for this analysis are presented in Table 2 [26,27].

**Table 1.** Material properties of the heat exchanger.

| Material | Elastic modulus (GPa) | Mass density ($kg/m^3$) | Thermal conductivity (W/(m·K)) | Specific heat (J/(kg·K)) |
|---|---|---|---|---|
| Copper | 101 | 8933 | 401 | 385 |
| Stainless steel | 193 | 7900 | 14.9 | 477 |
| Carbon steel | 200 | 7854 | 60.5 | 434 |
| Titanium | 120 | 4500 | 21.9 | 522 |

**Table 2.** Hybrid nanofluid properties of the heat exchanger.

| Nanofluid | Thermal conductivity (W/(m·K)) | Density ($g/cm^3$) | Specific heat (J/(kg·K)) | Viscosity (Pa·s) |
|---|---|---|---|---|
| Water | 0.31 | 0.998 | 4180 | 0.000797 |
| CuO-ZnO-Water | 0.61 | 1.0745 | 4141.58 | 0.000816925 |
| EG-Water | 0.349 | 1.08627 | 3084 | 0.00538 |
| CuO-EG-Water | 0.359 | 1.13851 | 2942.61 | 0.00615 |
| $SiO_2$-EG-Water | 0.381 | 1.15429 | 2814.09 | 0.00758 |
| $Al_2O_3$-EG-Water | 0.425 | 1.25929 | 2645.35 | 0.00967 |

### *2.3. Mesh optimization*

Establishing an optimal mesh for the shell and tube heat exchanger is a crucial step for ongoing simulations and analysis of this research. The validation outcomes, detailed in Figure 2, involved reducing the mesh size, and thus increasing the number of elements, for several run iterations until obtaining same outcomes regardless of changing the mesh size, i.e. the model outcomes become independent of the mesh size. Total of eight trials with different mesh sizes were adopted, as illustrated in Figure 2, to obtain outcomes that were independent of the mesh size. Once mesh optimization obtained, model outcomes were compared with experimental data. However, finer meshes demand more time for computation. After extensive analysis and multiple simulations, the optimal mesh of the model, identified as the fifth iteration data point in Figure 2, consisted of 986,362 elements, holding consistency across all simulations in this study.

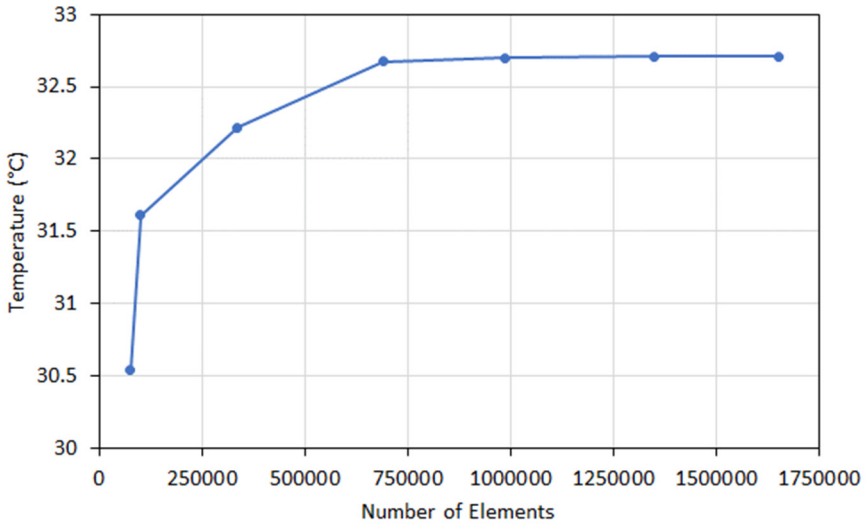


**Figure 2.** Mesh optimization: fluid outlet temperature vs. number of elements.

*2.4. Simulation validation*

The numerical model is compared with experimental data to validate the simulation outcomes without implementing any correction factors. Consequently, the validated model can be utilized to explore other types of nanofluids efficiently. The outlet temperature of the coolant fluid across different velocities was used to compare the numerical data with the experiments [27]. The outcomes with two distinct data are presented in Figure 3. To ensure accuracy, the simulation input variables were adjusted to align with the experimental research parameters, facilitating a comprehensive analysis of the system. The parameters and conditions used in this validation were based on having the inlet temperature for the coolant nanofluid and the hot fluid at 30 and 60 °C, respectively. All design and pressure parameters of the experiment were adopted in the development of the simulation and presented in the overall design and attribute section and model simulations section of this paper. This validation approach involves examining the overall temperature change associated with coolant nanofluid without altering variables or incorporating any correction factors. This examination revealed similar temperature changes that align with the corresponding compared findings. The degree of agreement between numerical and experimental results was within an average of 1.8% across the entire range of the explored velocities. This validation process verified the accuracy of the shell and tube heat exchanger analysis and simulations concerning this study.

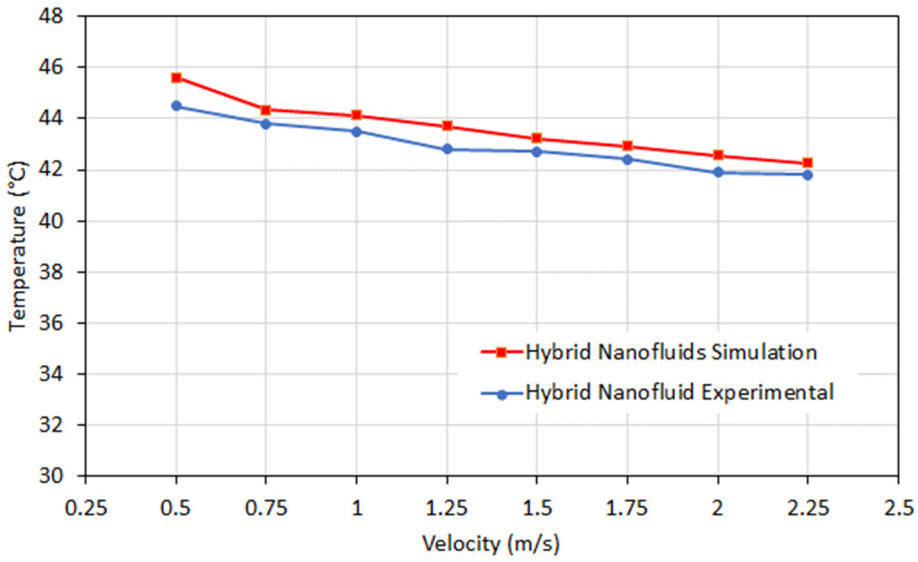


**Figure 3.** Comparison of experimental and simulated models for a heat exchanger utilizing hybrid nanofluids.

*2.5. Model simulations*

Since our main focus was to optimize the cooling nanofluids for optimal heat exchanger performance, the simulations were configured to emulate a steady-state, fully developed flow, maintaining identical inlet mass flow rates of 0.01 kg/s, albeit differing in temperature and fluid properties. Eight distinct inlet velocities were tested for both the coolant nanofluid and the hot fluid: 0.50, 0.75, 1.00, 1.25, 1.50, 1.75, 2.00 and 2.25 m/s. These velocities were applied individually to the inlets of both the coolant nanofluid and the hot fluid. Water was designated as the hot fluid; while the coolant nanofluid encompassed five different nanofluids: CuO-ZnO-Water, EG-Water, CuO-EG-Water, $SiO_2$-EG-Water, and $Al_2O_3$-EG-Water. Each of these five coolant nanofluids underwent analysis at the eight specified velocities. Moreover, the inlet temperature for the coolant nanofluid was set at 30 ℃, whereas the hot fluid consistently entered at 60 ℃ [27–29]. Furthermore, the outlets for both the coolant and hot fluids were established as open boundaries, subject to atmospheric parameter with a pressure of 101325 Pa to simulate real-world conditions. Figure 4 visually illustrates the fluid subdomains pertinent to the shell and tube heat exchanger system. In Figure 4a, the coolant nanofluid subdomain was contained within the tubes and headers of the system, while in Figure 4b, the hot fluid subdomain was confined within the shell of the system.

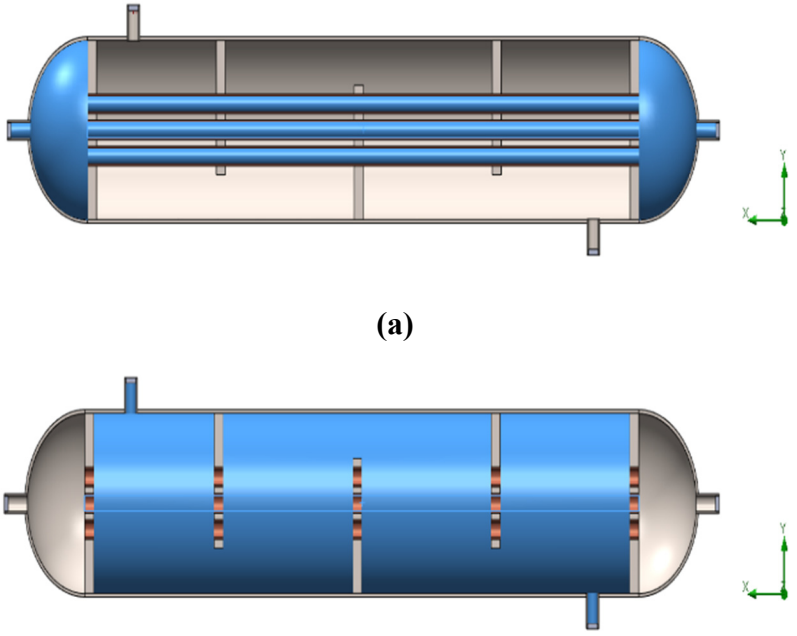

**(a)**

**(b)**

**Figure 4.** Fluid subdomains: (a) coolant nanofluid, (b) hot fluid.

## 3. Results and discussion

The data derived from the experimentally validated models involving five distinct coolant nanofluids and their respective velocities are presented in Tables 3 and 4. Tabulating this data facilitated a comprehensive examination to determine the optimal nanofluid for temperature variation at particular velocity values. Specifically, Table 3 displays the outlet temperatures of the coolant nanofluids, while Table Table 4 depicts the outlet temperatures of the hot fluids corresponding to the utilized coolant nanofluids and velocities. The data from these tables was visualized in Figures 5 and 6, offering a more insightful representation of nanofluids behavior.

Notably, an immediate observation was the inverse relationship between fluid velocity and outlet temperature in Figure 5, resulting in a diminished temperature change. Moreover, Figure 6 illustrates the hot fluid's outlet temperature concerning the corresponding coolant nanofluids and different inlet velocities. The findings mirrored those from Figure 5, highlighting analogous trends in temperature alteration. These results corroborated initial hypotheses regarding temperature distribution, grounded in Newton's 2nd Law of Cooling. Hence, the process of determining the optimal coolant nanofluid centered on identifying the nanofluid that induced the most significant temperature change across all fluid velocities. This comparative analysis revealed that among the five coolant nanofluids, CuO-ZnO-Water exhibited the most efficient performance by consistently reducing the hot fluid's temperature across all velocities. The exceptional properties and thermal conductivity of CuO-ZnO-Water compared with the other hybrid nanofluids played significant role in achieving those outcomes. Calculations, based on a coolant nanofluid inlet temperature of 30 °C, revealed the most substantial temperature change throughout the system occurred at a velocity of 0.50 m/s when employing CuO-ZnO-Water as the coolant nanofluid. Additionally, Figures 5 and 6 illustrate that the most substantial temperature

reductions in the hot fluids occurred during slower velocities. It was observed that the average temperature reduction in the outlet fluids using CuO-ZnO-Water as a coolant hybrid nanofluid was enhanced by over 9% compared with approximately 6% in the other hybrid nanofluids at a low velocity of 0.5 m/s. In contrast, at the higher velocity of 2.25 m/s, there was an average enhancement of over 5% with the use of CuO-ZnO-Water, while only around half of this improvement was presented with the implementation of the other nanofluids. This observation suggested that analyzing slower fluid velocities would likely result in more pronounced temperature changes.

**Table 3.** Coolant nanofluids tube outlet temperatures (°C).

| Velocity (m/s) | CuO-ZnO-Water | EG-Water | CuO-EG-Water | $SiO_2$-EG-Water | $Al_2O_3$-EG-Water |
|---|---|---|---|---|---|
| 0.50 | 35.15 | 34.75 | 34.83 | 35.05 | 35.13 |
| 0.75 | 34.22 | 33.92 | 33.88 | 34.08 | 34.11 |
| 1.00 | 33.69 | 33.17 | 33.21 | 33.46 | 33.54 |
| 1.25 | 33.47 | 32.76 | 32.77 | 32.92 | 33.07 |
| 1.50 | 33.25 | 32.53 | 32.51 | 32.58 | 32.67 |
| 1.75 | 33.16 | 32.33 | 32.34 | 32.37 | 32.42 |
| 2.00 | 33.14 | 32.22 | 32.19 | 32.25 | 32.23 |
| 2.25 | 33.12 | 32.11 | 32.08 | 32.11 | 32.11 |

**Table 4.** Hot fluids shell outlet temperatures (°C) corresponding to coolant nanofluids.

| Velocity (m/s) | CuO-ZnO-Water | EG-Water | CuO-EG-Water | $SiO_2$-EG-Water | $Al_2O_3$-EG-Water |
|---|---|---|---|---|---|
| 0.50 | 54.57 | 56.25 | 56.22 | 56.09 | 55.93 |
| 0.75 | 55.62 | 56.99 | 56.96 | 56.93 | 56.79 |
| 1.00 | 56.26 | 57.57 | 57.51 | 57.41 | 57.27 |
| 1.25 | 56.61 | 57.88 | 57.86 | 57.81 | 57.62 |
| 1.50 | 56.76 | 58.03 | 58.12 | 58.05 | 57.95 |
| 1.75 | 56.95 | 58.19 | 58.19 | 58.19 | 58.14 |
| 2.00 | 56.91 | 58.31 | 58.29 | 58.32 | 58.33 |
| 2.25 | 56.89 | 58.45 | 58.43 | 58.39 | 58.37 |

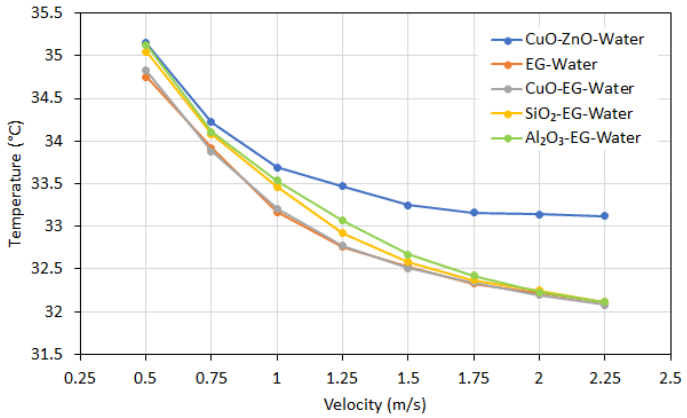


**Figure 5.** Temperatures of coolant nanofluids at tube outlet vs. velocity.

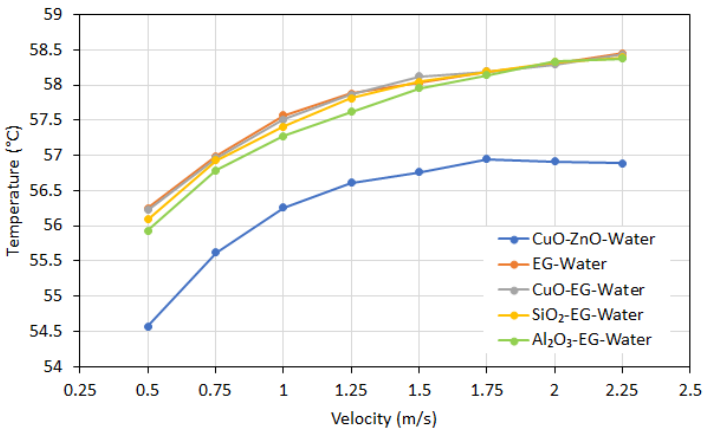


**Figure 6.** Temperatures of hot fluids at shell outlet in relative to coolant nanofluids vs. velocity.

Moreover, by plotting the flow trajectory lines depicting the temperature distribution as the fluids traversed through the system at three specific inlet fluid velocities (0.5, 1.5, and 2.25), as illustrated in Figures 7–9 respectively, valuable insights were seen. These figures elucidated the fluid flow patterns within the system and identified potential design alterations that could heighten the overall thermal efficiency. Each figure correlated with an inlet velocity that manifested the most pronounced temperature alteration. Markedly, Figures 7–9 denoted between a–e, representing the five distinct coolant nanofluids under analysis. The latter figures consistently depicted CuO-ZnO-Water, in Figure 7a, 8a, and 9a, exhibiting the most substantial temperature variation compared to other nanofluids. An evident inference drawn from these graphical representations suggested that revising the heat exchanger design by relocating the shell outlet to the top of the system could reduce the hot fluid's outlet temperature. This re-design allows an additional fluid pass around the coolant pipes, and thus permit further heat exchange before exiting the system. Alternatively, retaining the current placement of the shell outlet would necessitate adjusting the baffle spacing by shortening it and introducing an additional baffle to enable a secondary passage of the fluid, thereby potentially enhancing efficiency.

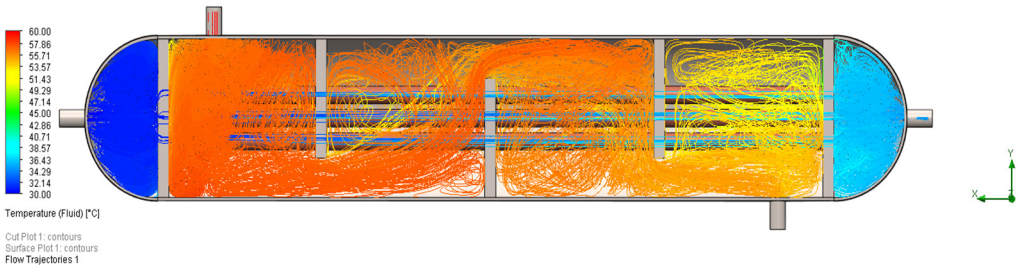


**(a)**

*Continued on next page*

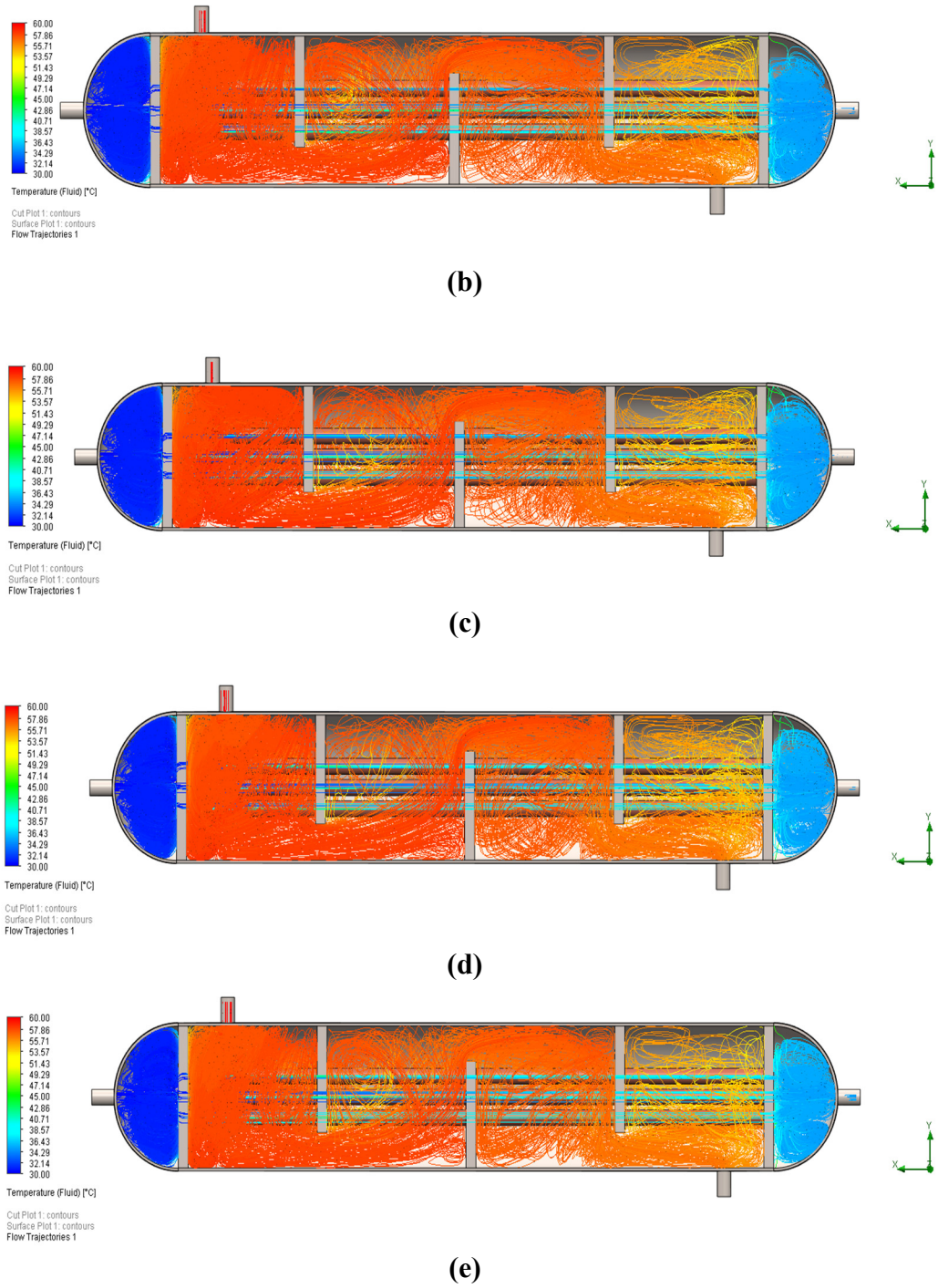


**Figure 7.** Temperature flow trajectory lines for various coolant nanofluids at 0.5 m/s: (a) CuO-ZnO-Water, (b) EG-Water, (c) CuO-EG-Water, (d) $SiO_2$-EG-Water, and (e) $Al_2O_3$-EG-Water.

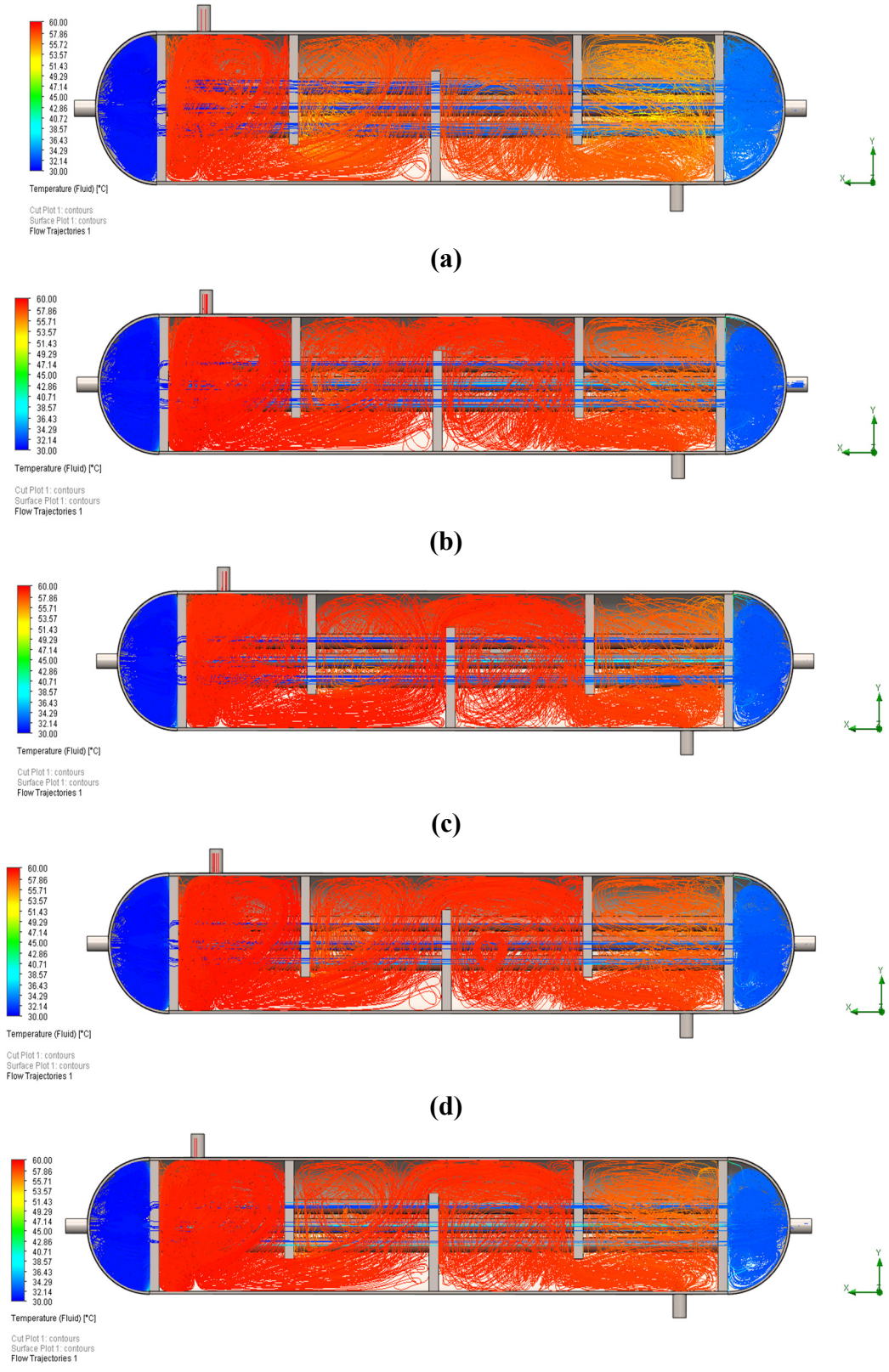


**Figure 8.** Temperature flow trajectory lines for various coolant nanofluids at 1.5 m/s: (a) CuO-ZnO-Water, (b) EG-Water, (c) CuO-EG-Water, (d) $SiO_2$-EG-Water, and (e) $Al_2O_3$-EG-Water.

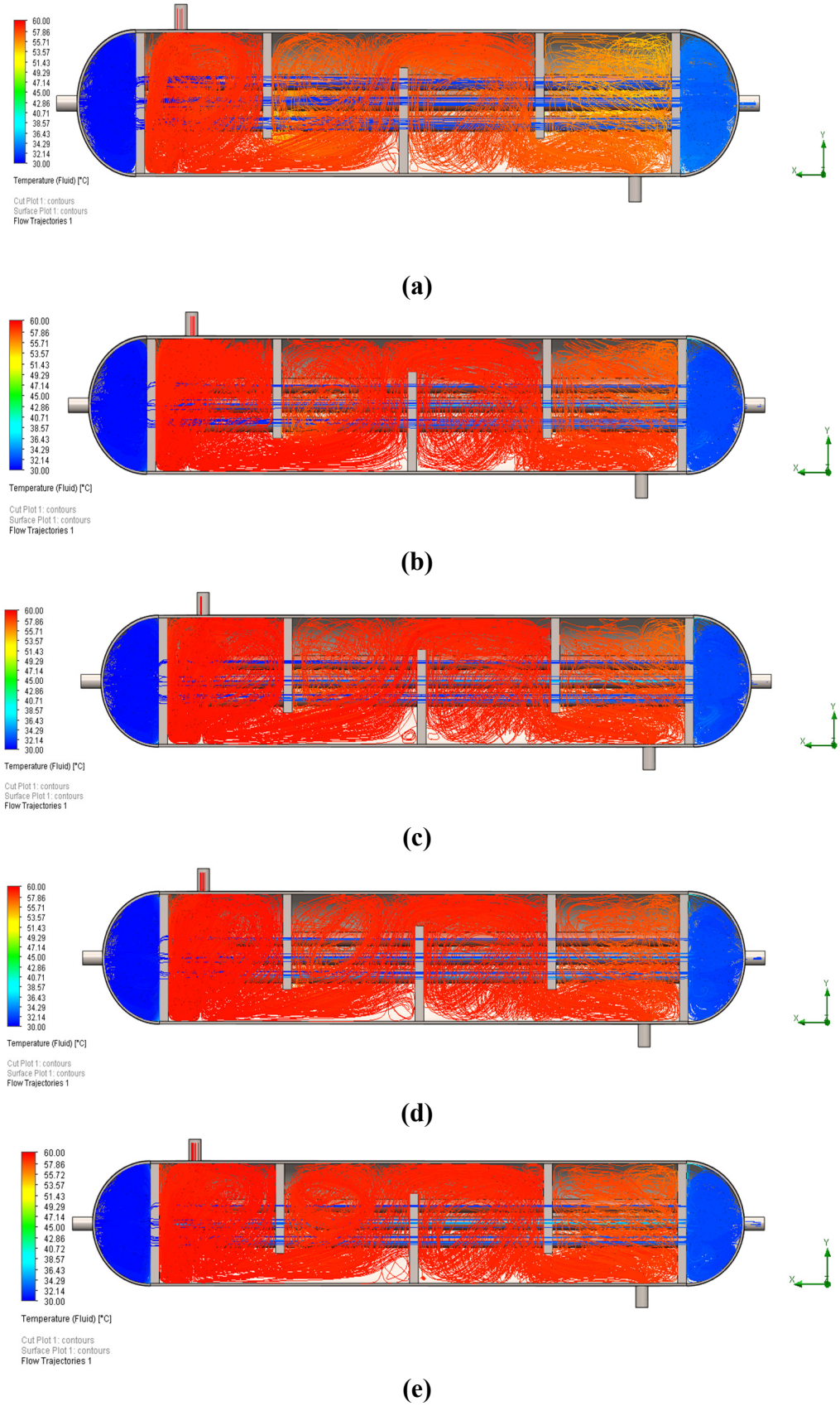


**Figure 9.** Temperature flow trajectory lines for various coolant nanofluids at 2.25 m/s: (a) CuO-ZnO-Water, (b) EG-Water, (c) CuO-EG-Water, (d) $SiO_2$-EG-Water, and (e) $Al_2O_3$-EG-Water.

In addition to identifying the optimal nanofluids, it is curial to optimize the material type of heat exchanger as it also plays significant role in enhancing heat transfer of system alongside the coolants. Several analyses were conducted on various materials utilized for the tubing to optimize the outstanding option. The characteristics of copper and three other main materials utilized for tubing were tabulated in Table 1. Subsequently, Figure 10a illustrates the outlet temperature of the coolant hybrid nanofluid at various velocities, while Figure 10b depicts the outlet temperature of the hot fluid with the increased velocity for the four different materials. Throughout these simulations, the inlet temperature of the coolant nanofluid stood at 30 ℃, while the inlet temperature of the hot fluid remained at 60 ℃, with the coolant nanofluid chosen as $Al_2O_3$-EG-Water and the hot fluid as water. The outcomes revealed that copper emerged as the optimal tubing material, inducing the most significant temperature change throughout the system. Additionally, as the fluid's velocity exceeded 2.0 m/s, the four diverse materials began yielding similar outcomes. This could be attributed to the limited contact time between the fluid and the heat transfer surface at high velocities. This limited contact time weakens the correlation between heat transfer and the material properties of the surface. At these speeds, the fluid spends less time in contact with the heat transfer surface. This reduces the overall heat transfer coefficient, which serves as the key parameter for determining heat transfer [24]. Based on the fluid velocity findings, the material that induced the most substantial temperature change at a lower velocity appeared more advantageous. Consequently, considering the results and supplementary simulations outcomes for the heat exchanger materials and nanofluids types, the analysis culminated in the determination that a shell and tube heat exchanger employing copper as the tubing material, paired with CuO-ZnO-Water as the coolant nanofluid, presented the most efficient heat exchange system in this study.

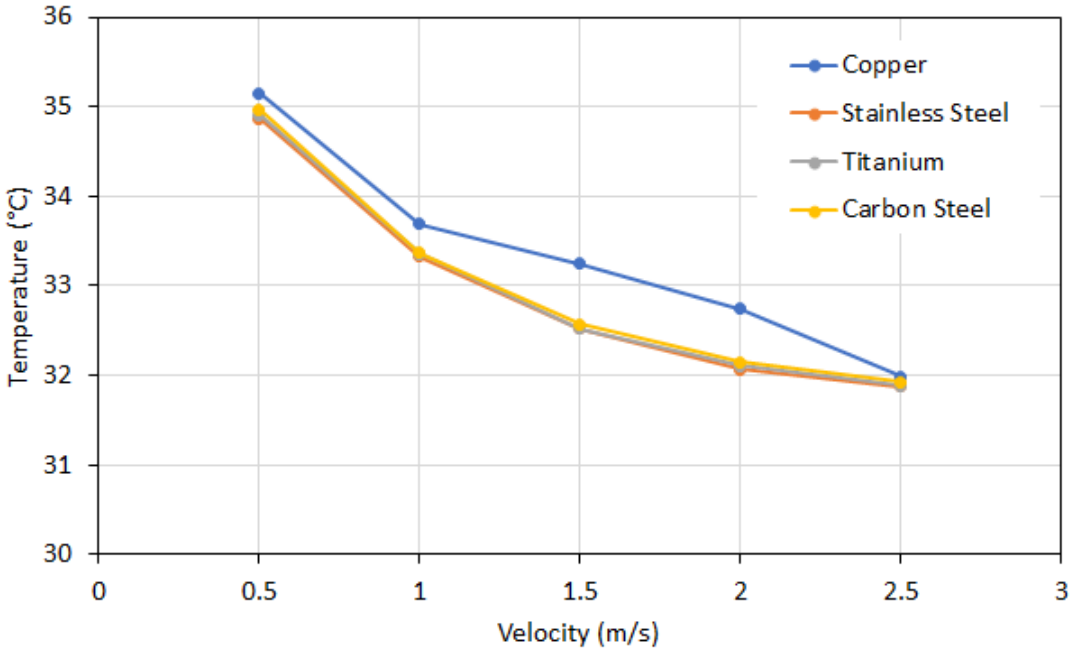


**(a)**

*Continued on next page*

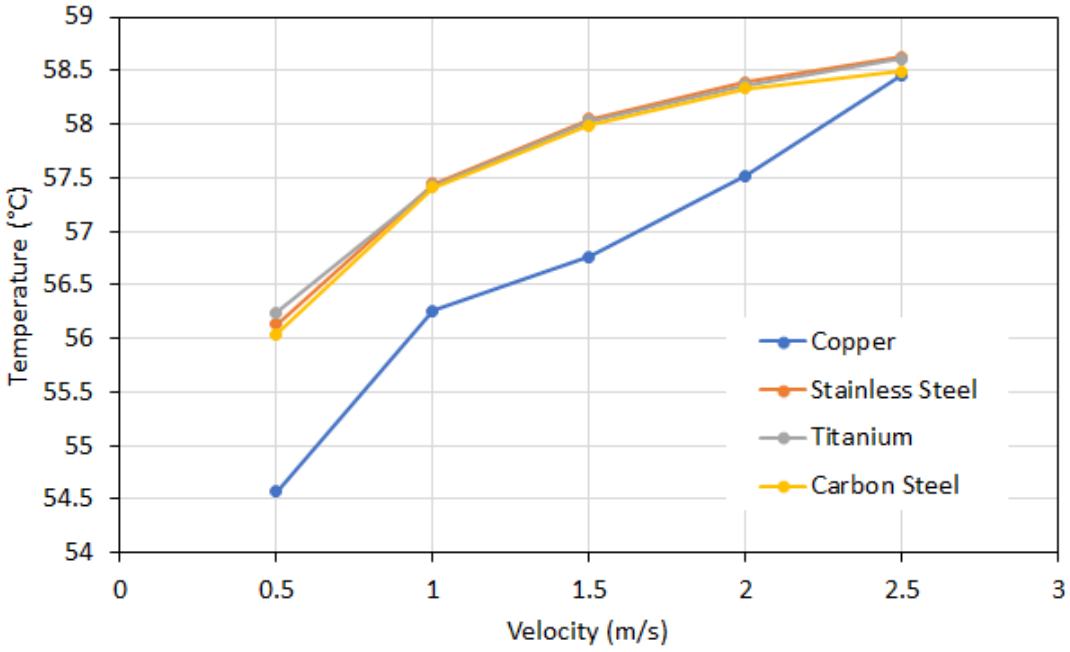


**(b)**

**Figure 10.** Temperature vs. velocity for various tubing materials: (a) outlet temperature of coolant nanofluid, (b) outlet temperature of hot fluid.

Since the previous results indicated that CuO-ZnO-Water is the outstanding candidate among other hybrid nanofluids, further analysis were obtained to evaluate the performance of this nanofluid utilizing Eqs (1) and (2) to calculate Reynolds number ($R_e$) and Prandtl number ($P_r$) of both the base fluid and the nanofluid [30,31]:

$$R_e = \frac{\rho\, v\, D}{\mu} \tag{1}$$

$$P_r = \frac{\mu\, c_p}{K} \tag{2}$$

where: $\rho$ = density (kg/m$^3$), $v$ = velocity (m/s), $D$ = diameter (m), $\mu$ = viscosity (kg/(m·s)), $c_p$ = specific heat (J/(kg·K)), and $K$ = thermal conductivity (W/(m·K)).

Additionally, the computation of friction factor and Nusselt number exclusively for the base fluid has been executed utilizing the Gnielinski equation [32], recognized for its suitability in turbulent flow conditions. Hence, Eq (3) can be utilized to compute the friction factor ($f$) pertaining to the base fluid:

$$f = [1.58\ \ln R_e - 3.82]^{-2} \tag{3}$$

The Nusselt number ($N_u$) can be calculated for the base fluid from the turbulent flow using Eq (4):

$$N_u = \frac{(0.125f)(R_e - 1000)P_r}{1+12.7(0.125f)^{0.5}\,(P_r{}^{2/3}-1)} \tag{4}$$

Notwithstanding, the friction factor for a flow rate with nanoparticles can be determined using the correlation proposed by Duangthongsuk and Wongwises [33] , as the Gnielinski equation [32] for

single-phase flow cannot be applied to compute the friction factor and Nusselt number. It is important to acknowledge that this equation is specifically applicable to turbulent flow conditions and is unsuitable for laminar flow conditions [29]. Hence, Eq (5) can be used to determine the friction factor ($f$) regarding the nanofluid:

$$f = 0.961\, {R_e}^{-0.375}\, \emptyset^{0.052} \tag{5}$$

where $\emptyset$ = volume concentration (%).

The calculation of the Nusselt number ($N_u$) for the nanofluid is determined using the correlation established by Duangthongsuk and Wongwises for turbulent flow [33,34], as per Eq (6):

$$N_u = 0.074\, {R_e}^{0.707}\, {P_r}^{0.385}\, \emptyset^{0.074} \tag{6}$$

The determination of the friction factor within nanofluid under turbulent flow conditions is achieved through the utilization of Eq (5). Figure 11 illustrates the relationship between the friction factor and Reynolds number. Observations reveal a decline in the friction factor as the Reynolds number increases. The decline percentage of the friction factor was 43% for Reynolds number ranging approximately from 10,000 to 40,000. This decrease in the friction factor is associated with the reduction in the thickness of the hydraulic boundary layer, a phenomenon that occurs as the Reynolds number increases [35].

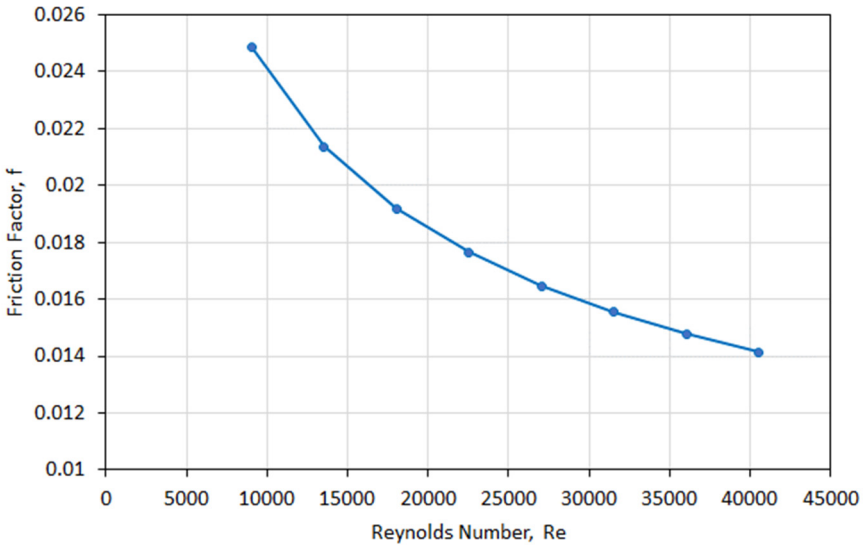


**Figure 11.** Friction factor vs. Reynolds number for CuO-ZnO-Water nanofluid.

The modification of the base water by adding nanoparticles has notably transformed the thermophysical properties of the nanofluid. The variation of the Nusselt number against Reynolds number is depicted in Figure 12, ranging approximately from 10,000 to 40,000 for both the nanofluid and the base water. It is evident that the Nusselt numbers of the nanofluid exhibited further increases across all Reynolds numbers compared to those of the base fluid (water). Utilizing nanofluid as the working fluid within a shell and tube heat exchanger results in not only an increase in the Nusselt number but also a reduction in temperature as the Reynolds number increases, as demonstrated in Figure 13. These outcomes are attributed to the increased random and chaotic movements, collisions,

and migration of nanoparticles within the suspension of the nanofluid, which intensify with the rise in mass flow rate. Consequently, this escalation enhances the turbulent intensity, leading to an improvement in heat transfer [36,37].

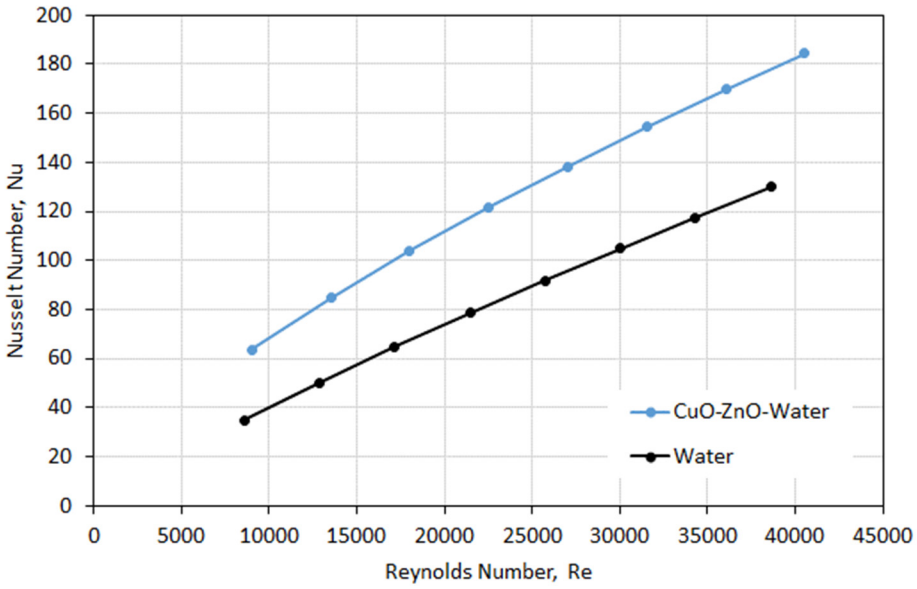


**Figure 12.** Nusselt number vs. Reynolds number for CuO-ZnO-Water nanofluid and the base fluid (water).

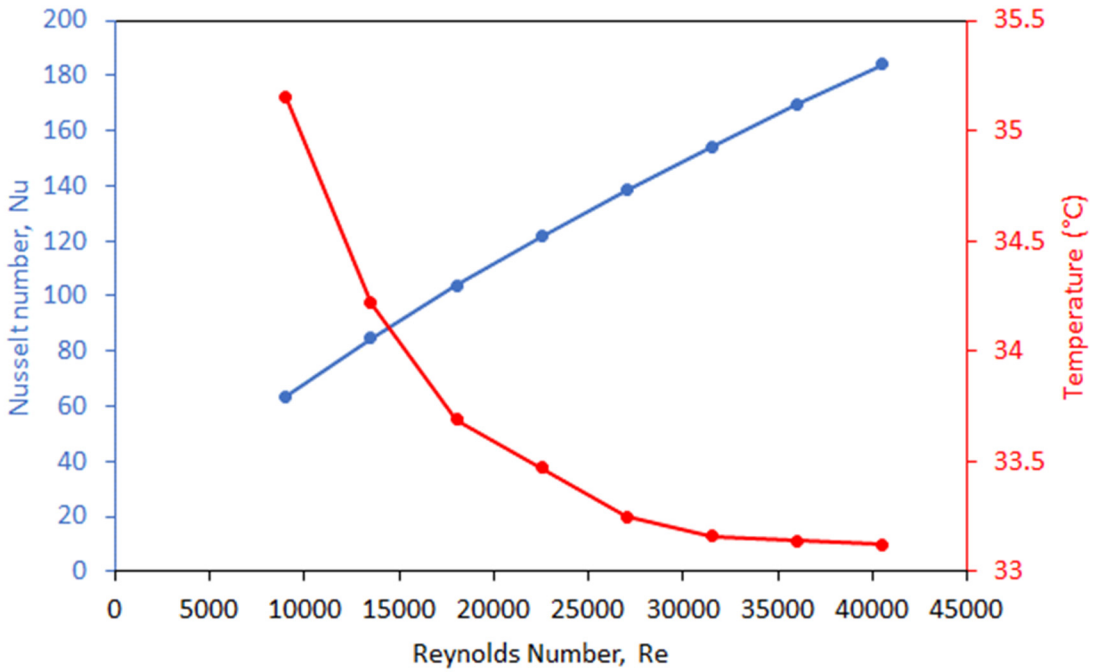


**Figure 13.** Variation of Nusselt number and temperature with Reynolds number.

## 4. Conclusions

Heat transfer performance in a shell and tube heat exchanger using various hybrid nanofluids (CuO-ZnO-Water, EG-Water, CuO-EG-Water, $SiO_2$-EG-Water, and $Al_2O_3$-EG-Water) under laminar and turbulent flow conditions was investigated in this study. After validating the numerical models with experimental test results, the validated models were developed to explore the influence of hybrid nanofluids and diverse materials on heat exchanger performance. The investigation revealed notable disparities in the efficacy of coolant hybrid nanofluids in reducing the average outlet fluid temperature. Specifically, when employing CuO-ZnO-Water as a coolant, a substantial increase of over 9% in temperature reduction was observed, as opposed to the approximately 6% attained by other hybrid nanofluids at a lower velocity of 0.5 m/s. Conversely, at a higher velocity of 2.25 m/s, the utilization of CuO-ZnO-Water led to an average enhancement of over 5% in temperature reduction. Comparatively, the implementation of alternative nanofluids yielded only about half of this improvement under similar conditions. The findings of these investigations led to the determination that, among the configurations studied, a shell and tube heat exchanger employing copper as the tubing material in conjunction with CuO-ZnO-Water as the coolant hybrid nanofluid exhibited the most efficient heat exchange system. The outcomes derived from this study also indicated that lower inlet velocities for the fluids generated a more pronounced temperature alteration, directly elevating the system's thermal efficiency.

Moreover, the investigation evaluated the impact of Reynolds number pertaining to the hybrid nanofluid on the Nusselt number ($N_u$) and friction factor ($f$). The results indicated the superior heat transfer capabilities of the hybrid nanofluid compared to the base fluid across all conditions. Notably, higher Reynolds numbers corresponded to increased $N_u$ values and decreased friction factors ($f$).

These outcomes indicated a significant enhancement in heat transfer performance within the heat exchanger due to the incorporation of nanoparticles in the base fluid. The increased Nusselt numbers and reduced friction factors were attributed to the modified thermophysical properties of the nanofluid. Furthermore, we emphasized the necessity of optimizing nanoparticle types for the creation of hybrid nanofluids, particularly in improving industrial heat exchangers and their coolant performance. We recommend extending this study in the future by delving into the properties of novel nanoparticles across different mass fractions within the hybrid nanofluids. Additionally, expanding the scope to encompass an analysis of the influence of hybrid nanofluids on diverse types of heat exchangers would be beneficial. The implementation of hybrid nanofluids as working fluids in shell and tube heat exchangers can markedly enhance the performance of these systems. This enhancement plays a pivotal role in various components, encompassing intercoolers, boilers, pre-heaters, and condensers within power plants. Furthermore, their utilization extends beyond power plants to include biomass heating plants and numerous other engineering processes. Ultimately, the utilization of hybrid nanofluids along with flow simulation yielded valuable insights into investigating optimal shell and tube heat exchanger configurations.

## Use of AI tools declaration

The author declare that they have not used Artificial Intelligence (AI) tools in the creation of this article.

## Conflict of interest

The authors declare no conflicts of interest.

## References


1. Mohammadi MH, Abbasi HR, Yavarinasab A, et al. (2020) Thermal optimization of shell and tube heat exchanger using porous baffles. *Appl Therm Eng* 170: 115005. https://doi.org/10.1016/j.applthermaleng.2020.115005
2. Edreis E, Petrov A (2020) Types of heat exchangers in industry, their advantages and disadvantages, and the study of their parameters. *IOP Conf Ser: Mater Sci Eng* 963: 012027. https://doi.org/10.1088/1757-899X/963/1/012027
3. Smith R, Pan M, Bulatov I (2013) 32-Heat transfer enhancement in heat exchanger networks. In: Klemeš, Jiří J., *Handbook of Process Integration (PI),* Woodhead Publishing Series in Energy, 966–1037. https://doi.org/10.1533/9780857097255.5.966
4. Di Pretoro A, D'Iglio F, Manenti F (2021) Optimal cleaning cycle scheduling under uncertain conditions: A flexibility analysis on heat exchanger fouling. *Processes* 9: 93. https://doi.org/10.3390/pr9010093
5. Arsenyeva O, Orosz Á, Friedler F (2021) Retrofit synthesis of industrial heat exchanger networks with different types of heat exchangers. *Chem Eng Trans* 88: 613–618. https://doi.org/10.3303/CET2188102
6. Mehrjardi SAA, Khademi A, Said Z, et al. (2023) Effect of elliptical dimples on heat transfer performance in a shell and tube heat exchanger. *Heat Mass Transf* 59: 1781–1791. https://doi.org/10.1007/s00231-023-03367-7
7. Bejan A (1982) Entropy generation through heat and fluid flow. 1st Edition, John Wiley & Sons.
8. Bejan A, Tsatsaronis G, Moran MJ (1996) Thermal design and optimization. John Wiley & Sons.
9. Vivekh P, Bui DT, Islam MR, et al. (2020) Experimental performance evaluation of desiccant coated heat exchangers from a combined first and second law of thermodynamics perspective. *Energy Convers Manag* 207: 112518. https://doi.org/10.1016/j.enconman.2020.112518
10. Agyenim F, Eames P, Smyth M (2009) A comparison of heat transfer enhancement in a medium temperature thermal energy storage heat exchanger using fins. *Sol Energy* 83: 1509–1520. https://doi.org/10.1016/j.solener.2009.04.007
11. Sahin B, Demir A (2008) Performance analysis of a heat exchanger having perforated square fins. *Appl Therm Eng* 28: 621–632. https://doi.org/10.1016/j.applthermaleng.2007.04.003
12. Craig S, Grinham J (2017) Breathing walls: The design of porous materials for heat exchange and decentralized ventilation. *Energy Build* 149: 246–259. https://doi.org/10.1016/j.enbuild.2017.05.036
13. Dehghan M, Valipour MS, Saedodin S (2016) Microchannels enhanced by porous materials: Heat transfer enhancement or pressure drop increment? *Energy Convers Manag* 110: 22–32. https://doi.org/10.1016/j.enconman.2015.11.052
14. Yang J, Liu W (2015) Numerical investigation on a novel shell-and-tube heat exchanger with plate baffles and experimental validation. *Energy Convers Manag* 101: 689–696. https://doi.org/10.1016/j.enconman.2015.05.066

15. Nanan K, Thianpong C, Pimsarn M, et al. (2017) Flow and thermal mechanisms in a heat exchanger tube inserted with twisted cross-baffle turbulators. *Appl Therm Eng* 114: 130–147. https://doi.org/10.1016/j.applthermaleng.2016.11.153
16. Tawfik MA, Kadhim ZK, Hammoudi RY (2009) Vibration analysis of sudden enlargement pipe conveying fluid with presence of heat flux. *Eng Technol* 27: 533–557. https://doi.org/10.30684/etj.27.3.10
17. Geete A, Pathak R (2019) Effect of surface roughness on the performance of heat exchanger. *SN Appl Sci* 1: 901. https://doi.org/10.1007/s42452-019-0954-x
18. Attalla M, Maghrabie HM (2020) Investigation of effectiveness and pumping power of plate heat exchanger with rough surface. *Chem Eng Sci* 211: 115277. https://doi.org/10.1016/j.ces.2019.115277
19. Kumar V, Tiwari AK, Ghosh SK (2015) Application of nanofluids in plate heat exchanger: A review. *Energy Convers Manag* 105: 1017–1036. https://doi.org/10.1016/j.enconman.2015.08.053
20. Tiwari AK, Ghosh P, Sarkar J (2013) Performance comparison of the plate heat exchanger using different nanofluids. *Exp Therm Fluid Sci* 49: 141–151. https://doi.org/10.1016/j.expthermflusci.2013.04.012
21. Sivashanmugam P (2012) Application of nanofluids in heat transfer. In *An Overview of Heat Transfer Phenomena*, 16. https://doi.org/10.5772/52496
22. Kumar N, Urkude N, Sonawane SS, et al. (2018) Experimental study on pool boiling and critical heat flux enhancement of metal oxides based nanofluid. *Int Commun Heat Mass Transf* 96: 37–42. https://doi.org/10.1016/j.icheatmasstransfer.2018.05.018
23. Malika M, Sonawane SS (2021) The sono-photocatalytic performance of a novel water based $Ti^{+4}$ coated Al(OH)3-MWCNT's hybrid nanofluid for dye fragmentation. *Int J Chem React Eng* 19: 901–912. https://doi.org/10.1515/ijcre-2021-0092
24. Bergman TL, Lavine AS (2017) Fundamentals of heat and mass transfer. 8th ed. John Wiley & Sons.
25. Hibbeler RC (2016) Mechanics of materials. 10th ed. Pearson.
26. Namburu PK, Das DK, Tanguturi KM, et al. (2009) Numerical study of turbulent flow and heat transfer characteristics of nanofluids considering variable properties. *Int J Therm Sci* 48: 290–302. https://doi.org/10.1016/j.ijthermalsci.2008.01.001
27. Malika M, Bhad R, Sonawane SS (2021) ANSYS simulation study of a low volume fraction CuO-ZnO/Water hybrid nanofluid in a shell and tube heat exchanger. *J Indian Chem Soc* 98: 100200. https://doi.org/10.1016/j.jics.2021.100200
28. Zhou X, Wang Y, Zheng K, et al. (2019) Comparison of heat transfer performance of ZnO-PG, α-Al2O3-PG, and γ-Al2O3-PG nanofluids in car radiator. *Nanomater Nanotechnol* 9. https://doi.org/10.1177/1847980419876465
29. Radkar RN, Bhanvase BA, Barai DP, et al. (2019) Intensified convective heat transfer using ZnO nanofluids in heat exchanger with helical coiled geometry at constant wall temperature. *Mater Sci Energy Technol* 2: 161–170. https://doi.org/10.1016/j.mset.2019.01.007
30. Rott N (1990) Note on the history of the Reynolds number. *Annual review of fluid mechanics* 22: 1–12. https://doi.org/10.1146/annurev.fl.22.010190.000245
31. White FM (2006) Viscous fluid flow. 3rd ed., McGraw-Hill New York, 629.
32. Gnielinski V (1976) New equations for heat and mass transfer in turbulent pipe and channel flow. *Int J Chem Eng* 16: 359–367.

33. Duangthongsuk W, Wongwises S (2009) Heat transfer enhancement and pressure drop characteristics of $TiO_2$-water nanofluid in a double-tube counter flow heat exchanger. *Int J Heat Mass Transf* 52: 2059–2067. https://doi.org/10.1016/j.ijheatmasstransfer.2008.10.023
34. Albadr J (2018) Thermal performance of shell and tube heat exchanger using PG/Water and $Al_2O_3$ nanofluid. In *Advances in Heat Exchangers.* IntechOpen. https://doi.org/10.5772/intechopen.80082
35. Ahmed HE, Ahmed MI, Yusoff MZ (2015) Heat transfer enhancement in a triangular duct using compound nanofluids and turbulators. *Appl Therm Eng* 91: 191–201. https://doi.org/10.1016/j.applthermaleng.2015.07.061
36. Aminfar H, Motallebzadeh R (2012) Investigation of the velocity field and nanoparticle concentration distribution of nanofluid using Lagrangian-Eulerian approach. *J Dispers Sci Technol* 33: 155–163. https://doi.org/10.1080/01932691.2010.528336
37. Nourafkan E, Karimi G, Moradgholi J (2015) Experimental study of laminar convective heat transfer and pressure drop of cuprous oxide/water nanofluid inside a circular tube. *Exp Heat Transf* 28: 58–68. https://doi.org/10.1080/08916152.2013.803178


AIMS Press